RESEARCH ARTICLE

Effects of debris entrainment and recycling on explosive volcanic eruption jets and columns

Greg A. Valentine[1]

Abstract

A multiphase fluid dynamic model is used to explore the effects of entrainment of granular debris into sustained volcanic jets such as those which produce sub-Plinian to Plinian eruption columns. The debris may be sourced from processes such as avalanches from crater walls or from recycling of previously erupted material. The results indicate that debris is not immediately, homogeneously mixed into a jet but instead forms a dense sheath that is dragged upward around the jet margin. While very small volumes of debris relative to the eruptive discharge rate mix progressively into the jet with increasing altitude, the dense sheath can inhibit entrainment of air into the lower portions of the jet, which may explain signs of column instability such as increased stratification in fallout deposits where lithic content increases. As debris volume increases, the dense sheath can collapse from a range of elevations to feed pyroclastic currents. The presence of the sheath of entrained debris contradicts some assumptions such as the top-hat profile for density and velocity that is commonly used in 1-D models. Transitions from fallout-producing buoyant column to collapsing behavior can be related to debris entrainment without any changes in primary eruption parameters such as vent size, exit velocity, or gas content. Boiling-over behavior can also be caused by debris entrainment, including recycling of previously erupted material such as might occur in a crater with restricted outlet. When entrained debris is relatively fine-grained such that it can couple well with the erupting mixture, complex, highly transient overpressured jet processes can occur due to the pinching effect of debris flowing into the base of the jet. Increasingly coarse debris causes collimation of the jet within the sheath of entrained material. The results suggest that accounting for the effects of debris entrainment is likely important for theoretical assessment of many natural eruption sequences and for assessment of hazard scenarios for potential sub-Plinian to Plinian activity.

Keywords Eruption column · Pyroclastic deposit · Fallout deposit · Ignimbrite · Multiphase flow · Boiling-over eruption

Introduction

Entrainment of debris into sustained eruption jets as they emerge from their vents is evidenced by varying proportions of accessory lithic clasts in the resulting pyroclastic deposits. Such accessory lithic clasts, which for brevity in this paper are simply referred to as lithics, are found in the products of both fallout and pyroclastic currents. In Plinian and sub-Plinian fallout deposits, an increase in lithic abundance is often accompanied by increased stratification that indicates unsteady behavior in the parent eruption column (e.g., Walker 1981; Rosi et al. 1999; Taddeucci and Wohletz 2001; Scarpati and Perrotta 2016). Lithics in pyroclastic current deposits such as ignimbrites may be dispersed or concentrated into tuff breccia horizons that are a common proximal facies; the latter have been inferred to be related to debris introduced into eruptive jets causing a transition from buoyant to collapsing eruption columns and during the onset of caldera collapse (e.g., Druitt 1985; Druitt and Bacon 1986; Suzuki-Kamata et al. 1993; Bear et al. 2009; Simmons et al. 2016; Yasuda and Suzuki-Kamata 2018; Valentine et al. 2019). Proximal deposits, where exposed and accessible, show complex combinations of deposits from fallout and pyroclastic currents, and hybrids of the two, which may be coeval with more steady, buoyant behavior that produces relatively simpler fallout deposits in medial to distal reaches (e.g., Houghton et al. 2004; Di

✉ Greg A. Valentine
gav4@buffalo.edu

1   Department of Geology, University at Buffalo, Buffalo,
     NY 14260, USA

Muro et al. 2004, 2008; Hildreth and Fierstein 2012; Gilchrist and Jellinek 2021; Dowey and Williams 2022); this behavior may be partly attributable to interaction of eruptive jets with debris-filled vents. In addition to lithics, proximal deposits from early phases of an eruption can be entrained as debris into an eruption column, a process that might be especially important during caldera subsidence (e.g., Wilson and Walker 1985; Wilson and Hildreth 1997) and in eruptions from craters with restricted outlets. The above field observations point to an important role for entrained debris in eruptive jets and columns, whether the debris is sourced from failure of shallow conduit walls, from rockslides and avalanches originating at crater and/or caldera walls, or as recycled pyroclastic material.

Most models of eruption columns treat the discharge at vent as a homogeneous mixture with no time variation for sustained eruptions. This is largely a pragmatic approach due to the complexity of processes associated with eruption jets and columns even when the mixture discharging at the vent is assumed to be steady and uniform. One-dimensional, steady models with perfectly coupled gas-particle mixtures form the most common approach to eruption columns (e.g., Woods 1988; Glaze and Baloga 1996; Mastin 2007); these models assume that gas pressure within eruption columns is equal to that of the ambient atmosphere (pressure balanced) and treat mixture density at a given level as constant within the column (also referred to as a top-hat profile). Two- and three-dimensional, transient models do not impose particle concentration or velocity profiles on an eruption column, but the source discharge is typically treated as having homogeneous and steady velocity and particle concentration (e.g., pseudofluid model of Suzuki et al. 2005; Suzuki and Koyaguchi 2012; and multiphase models such as Valentine and Wohletz 1989; Neri and Dobran 1994; Carcano et al. 2014; Cerminara et al. 2016). Nevertheless, it is well known that steady, uniform flow of gas and particles is not the norm due to imperfect coupling between the two which leads to strong time and space variations in particle concentration and speed as a mixture ascends its conduit; this has been shown both experimentally and numerically (e.g., Anilkumar et al. 1993; Dartevelle and Valentine 2007). Addition of debris to the base of an erupting jet is another potential source of flow heterogeneity that has been little explored in the volcanology literature, and is the focus of this study.

Transitions in sustained eruptions from buoyant plumes with fallout to fountaining and pyroclastic currents are often related primarily to vent widening and/or volatile content changes, both of which affect exit speed and mass flux at the vent (e.g., Wilson and Sparks 1980; Sparks et al. 1997). Wide vents and/or low volatile contents (and low vent velocities) promote fountaining and pyroclastic currents, while narrower vents and high gas contents promote the formation of buoyant columns and fallout. Low eruption temperatures also promote fountaining relative to high temperatures, but this is usually a secondary effect in volatile-driven eruptions due to the relatively narrow range of likely magma temperatures. Suzuki and Koyaguchi (2012) further distinguished between collapse along the margins of erupting, pressure-balanced jets versus wholesale collapse to form fountain structures, complementing the results of Ogden et al. (2008) who showed complex, oscillating collapse dynamics for jets that exit the vent at pressures greater than that of the ambient atmosphere (overpressured, or underexpanded, jets). Gilchrist and Jellinek (2021) thoroughly reviewed previous field and fluid dynamic studies related to partial column collapse and provided new insights based upon analog experiments. Bear et al. (2009) and Simmons et al. (2016) inferred that overloading of eruption columns with entrained dense lithics contributed to column collapse and pyroclastic currents.

Here, I explore on the effects of debris entrainment on the low-altitude development of explosive eruption columns. I focus on general phenomenology of the process, rather than on quantitatively assessing specific eruption scenarios, with an emphasis on geological implications. Entrainment of debris into an erupting jet can have profound effects on its dynamics. Important impacts include (1) a dense (and cool) sheath that inhibits air entrainment and the transition to buoyancy; (2) simultaneous collapse of the outer portion of a jet and ascent of its inner portion; (3) promotion of boiling-over behavior; and (4) demonstration that the transition from buoyant to collapsing eruption columns can be related to debris influx without changes in primary eruption parameters. Debris entrainment is not necessarily a passive process wherein the material is immediately evenly dispersed into a jet such that it affects only the mixture's overall density.

Previous work and methods

The work presented here is part of a series of studies aimed at understanding interactions between debris and explosive volcanic processes within the framework of multiphase fluid dynamics. Sweeney and Valentine (2015) studied the effects of discrete subsurface explosions within debris-filled vents, including explosion-induced redistribution of subterranean materials. That work, which simulated expansion of a pressurized water vapor domain within initially stationary particle beds, was aimed at explaining field observations of phreatomagmatic vent structures (diatremes), in concert with experimental studies (Ross et al. 2008ab; Andrews et al. 2014, 2016; Graettinger et al. 2014; Valentine et al. 2014, 2015). Sweeney et al. (2018) modeled expansion of pressurized water vapor domains representing shallow phreatomagmatic explosions in upper portions of debris-filled diatremes, a few tens of meters beneath a crater floor, illustrating the

formation of pyroclastic currents and effects of topographically variable crater rim heights on the currents. Valentine and Cole (2021) extended the approach to study the effects of large, sustained eruptions penetrating their own fresh pyroclastic deposits as might occur in a caldera-forming eruption where pyroclastic currents pond within the subsiding depression. They demonstrated that entrainment of voluminous debris has profound effects on eruption jet (column) behavior even when the eruptive discharge is constant. The effects include development of pulsating overpressured jets (so-called gargling behavior; Wilson and Hildreth 1997) and multi-height collapse and feeding of pyroclastic currents from the margin of an eruption jet that, in the absence of entrained deposits, would otherwise be buoyant.

The approach I use here is similar to that of Valentine and Cole (2021) but is focused on smaller volumes of cold granular material such as would occur during crater wall avalanching or near-surface vent collapse. The multiphase approach solves conservation of mass, momentum, and specific internal energy for the gas (carrier phase) and particle fields (dispersed phase); governing equations are provided in the Appendix. Gas and particles are treated as overlapping continua within a control volume, which interact through momentum transfer (drag) and heat transfer (Syamlal et al. 2017; Valentine 2020). Additionally, multiple particle fields or classes, which can represent different particle properties such as diameter and/or density, exchange momentum with one another. Numerical solution is executed with the open source, finite volume code MFIX v. 20.3.1 (available at mfix. netl.doe.gov).
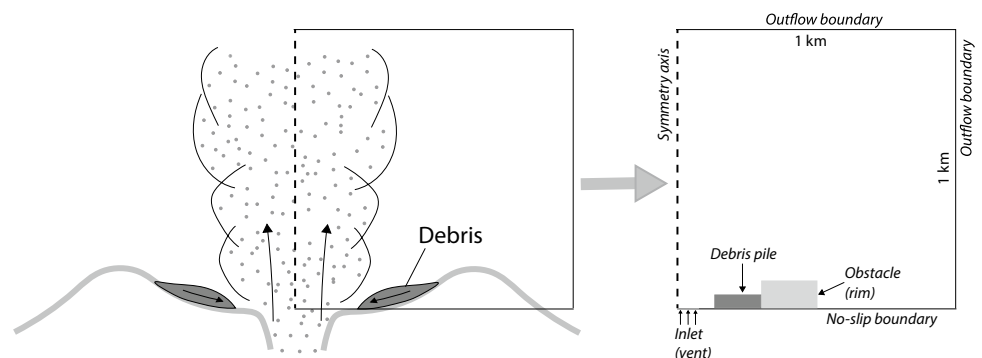
Simulations used a two-dimensional (2-D), axisymmetric domain that is a simple representation of a volcanic vent with a crater rim (Fig. 1). The domain has dimensions of 1 km × 1 km and a uniform grid resolution of 2.5 m (1.6×10^5 cells; Table 1). The grid resolution captures what can be a relatively narrow zone of initial interaction between the margin of an eruption jet and more concentrated debris, and is also intended to directly simulate the most important scales of turbulent mixing. 2-D simulations do not fully capture the complexity of turbulence structures,

compared to 3-D simulations (e.g., Suzuki et al. 2005), but are a necessary first step in understanding the interactions of debris with jets. The domain is filled with air that is stratified according to a standard atmospheric profile (with the base at sea level). All of the simulations feature an erupting mixture with 4 wt% water vapor, fine-ash size juvenile particles (0.1 mm diameter), and a constant velocity of 200 m/s maintained at the inlet to the computational domain (i.e., the vent; Table 1). These parameters correspond to a Mach number of ~ 1.4 for the exiting mixture, using a dusty-gas approximation (particles and gas in thermal and velocity equilibrium; Marble 1970). I anticipate that the results reported below are generally applicable to a range of Mach number conditions, because the primary driver of the phenomena of interest is the interaction between a vertical jet and an influx of high particle concentration debris with no initial vertical momentum. All of the modeled eruptive conditions are predicted to form buoyant columns, in the absence of any debris interaction, by the widely used, one-dimensional, steady-state model Plumeria (Mastin 2007). In most simulations, a debris "pile" is modeled in the cylindrical half-space as an anulus of initially stationary particles with a porosity of 0.4 and at or near ambient temperature (Fig. 1; note that I do not focus on temperature effects in this paper because particle concentrations play the dominant role). The debris particles have varying sizes and pile volumes (Table 2). The initial piles are set at some distance from the outer edge of the vent in most of the simulations in order to give the eruptive jet a short time interval to develop while the debris flows toward it.

Results

A series of runs involves vent radii of 25 m, yielding an eruptive dense-rock equivalent (DRE) volume flux of ~ 750 m^3/s (1.8×10^6 kg/s; Table 2). An eruptive discharge with no debris pile forms a simple jet with steady flow on average once its head exits the top of the domain (Fig. 2a); this serves as a reference for comparison with the effects of debris entrainment. Interaction of the jet with a 25-m-deep,

Fig. 1 Cartoon cross section of a natural eruption in a crater and an avalanche (lithic debris or previously erupted pyroclasts), next to the abstracted version used to set up the computational domain

Table 1 Initial and boundary conditions, and material properties common to all simulations[1]

Domain size (except run c2a2a)	1000 m high, 1000 m wide
Coordinate system	Cylindrical (axisymmetric)
Boundary conditions	
• Left side	• Symmetry axis
• Top	• Outflow
• Inlet	• Mass inflow (see below)
• Right side	• Outflow
• Bottom	• No slip wall (except inlet)
• Crater rim	• Free-slip block, left side at debris outer radius, width either 50 m or 100 m (height in Table 2)
Computational grid	Uniform, $\Delta r = \Delta z = 2.5$ m
Inlet (vent) condition (see also Table 2)	
• Gas	• H_2O
• Gas and particle temperature	• 900 °C
• Particle diameter	• 10^{-4} m
• Particle volume fraction	• 1.9×10^{-3}
• Water vapor content	• 4.0 wt%
• Vertical velocity	• 200 m/s
• Gas pressure	• 1.013×10^5 Pa
Debris initial conditions (see also Table 2)	
• Temperature	• Either 15 °C or 27 °C
• Void fraction	• 0.6
• Particle diameter	• 10^{-4}, 10^{-3}, or 10^{-2} m
Initial conditions outside debris pile	
• Gas	• Air
• Gas pressure	• Standard atmospheric pressure profile
• Temperature	• Standard atmospheric temperature profile
• Particle concentration	• Zero
• Gas properties (air and H_2O)	• Burcat and Ruscic (2005) thermochemical database. Approximated as air for thermal conductivity
Particle properties (juvenile and fill)	
• Density	• 2400 kg m^{-3}
• Heat capacity	• 1400 J kg^{-1} K^{-1}
• Coefficient of restitution	• 0.5
• Coefficient of friction	• 0.5
• Angle of internal friction	• 28°
• Maximum packing volume fraction	• 0.6

[1]The MFIX code has a "dilute threshold," the particle volume fraction below which the momentum equation for particle field is not solved and particle phase thermal conductivity is set to zero. The results reported here use the default value of 10^{-4} for the threshold.

15-m-wide debris pile (DRE volume of ~ 6×10^4 m³, equivalent to about 80 s of eruptive discharge) involves development of a dense (high particle concentration), cool sheath around the margin of the jet (see $t = 5$ s; Fig. 2b). This sheath is dragged upward by the jet core and, while it is diluted in the process, its high density promotes collapses along the jet margin from a range of heights (Fig. 2b; $t = 30$ and 60 s). This contrasts with a fountain-like collapse from a narrow range of heights that is common for jets where there is no interaction with debris but the mixtures fail to become buoyant (e.g., Valentine and Wohletz 1989; Neri and Dobran 1994; Valentine and Cole 2021). The different behavior here is related to the interior of the dense sheath interacting directly with the high-speed erupting mixture, while less momentum is imparted to the exterior of the sheath (Valentine and Cole 2021). The marginal collapses feed pyroclastic currents at ground level. A smaller debris pile, constituting ~ 1.2×10^4 m³, produces similar behavior (Fig. 2c); however, the debris volume is largely used up by 30 s, so that while marginal collapses have already begun to

Table 2 Simulation conditions[a]

Run	Vent radius (m)	Inner debris radius (m)	Outer debris radius (m)	Debris depth (m)	Debris particle diameter (m)	Rim height (m)	Debris volume, DRE[b] (m^3)	Volume flux at vent, DRE (m^3/s)	Particle classes
d1c	50	NA[c]	NA	NA	NA	NA	NA	3×10^3	1
d1ab	50	100	250	50	10^{-4}	50	4.9×10^6	3×10^3	2
d1ac	50	100	250	50	10^{-4}	50	4.9×10^6	3×10^3	1
d1ad	50	100	250	50	10^{-2}	50	4.9×10^6	3×10^3	2
d1b	50	50	100	50	10^{-4}	50	7.2×10^5	3×10^3	2
d1bb	50	50	100	50	10^{-2}	50	7.2×10^5	3×10^3	2
d1d	50	75	120	25	10^{-4}	50	4.1×10^5	3×10^3	1
d2	25	NA	NA	NA	NA	NA	NA	7.5×10^2	1
d2a	25	50	100	25	10^{-4}	50	3.5×10^5	7.5×10^2	2
d2a1	25	50	100	25	10^{-4}	50	3.5×10^5	7.5×10^2	1
d2b	25	50	100	25	10^{-2}	50	3.5×10^5	7.5×10^2	2
d2c	25	75	225	25	10^{-4}	50	2.1×10^6	7.5×10^2	1
d2d	25	50	100	25	10^{-3}	50	3.5×10^5	7.5×10^2	2
d2e	25	50	100	25	5×10^{-3}	50	3.5×10^5	7.5×10^2	2
d3a	25	35	50	25	10^{-4}	25	6.0×10^4	7.5×10^2	2
d3a1	25	35	50	25	10^{-4}	25	6.0×10^4	7.5×10^2	1
d3b	25	35	50	25	10^{-2}	25	6.0×10^4	7.5×10^2	2
d3c	25	35	50	25	10^{-3}	25	6.0×10^4	7.5×10^2	2
d4a	25	35	50	10	10^{-4}	25	2.4×10^4	7.5×10^2	2
d4a1	25	35	50	10	10^{-4}	10	2.4×10^4	7.5×10^2	2
d4b	25	35	50	10	10^{-3}	25	2.4×10^4	7.5×10^2	2
d5a	25	35	50	5	10^{-4}	25	1.2×10^4	7.5×10^2	2
d5a1	25	35	50	5	10^{-4}	5	1.2×10^4	7.5×10^2	2
d5a2	25	35	50	5	10^{-4}	25	1.2×10^4	7.5×10^2	1
d5b	25	35	50	5	10^{-3}	25	1.2×10^4	7.5×10^2	2
d5c	25	35	50	5	10^{-2}	25	1.2×10^4	7.5×10^2	2
d6a	100	NA	NA	NA	NA	NA	NA	1.2×10^4	1
d6b	100	105	120	5	10^{-3}	25	3.2×10^4	1.2×10^4	2
d6c	100	150	300	25	10^{-3}	50	3.2×10^6	1.2×10^4	2
d6d	100	150	300	25	10^{-4}	50	3.2×10^6	1.2×10^4	1

[a]The exit (vent) velocity for all simulations is 200 m/s, Mach number ~ 1.4 (mixture sound speed 147 m/s; Marble 1970)

[b]The debris volume is dense-rock equivalent (DRE) for an annulus defined by inner and outer radii and depth of debris

[c]*NA*, not applicable for simulations with no debris

occur, they are weaker, and soon after 60 s, in the upper few hundred meters of the domain, marginal collapse is declining in strength (Fig. 2c). This suggests that the jet is evolving toward the unimpeded behavior shown in Fig. 2a, although recycling of material that collapsed along jet margins back into the crater likely delays or may even prevent full recovery of free jet behavior. Comparison of simulations indicates that smaller debris volumes result in faster evolution of a jet toward unimpeded behavior, consistent with what would be intuitively expected. Very small volumes relative to the discharge rate do not produce collapses. For example, run d6b (Table 2) has a debris volume similar to run d5a2 (Fig. 2c), but with its larger vent and discharge rate, the

dense sheath is simply dragged up and progressively mixed by eddies into the jet core, without producing significant marginal collapses. The debris volume in d6b is equivalent to only ~ 3 s of the eruption discharge rate, while the debris volume for d5a2 is equivalent to ~ 16 s of eruption discharge.

Eruption jets with different vent radii (discharge rates) respond differently to similar debris volumes. Run d2a1 (Fig. 3a, Table 2) has a vent radius of 25 m and a pile volume of 3.5×10^5 m^3. It has the same vent size and conditions as the runs in Fig. 2b and c, but a larger debris volume. A dense sheath of debris is lifted along the jet margins, and the continuing supply of debris results in wholesale collapse. The eruptive jet has a complex and highly transient
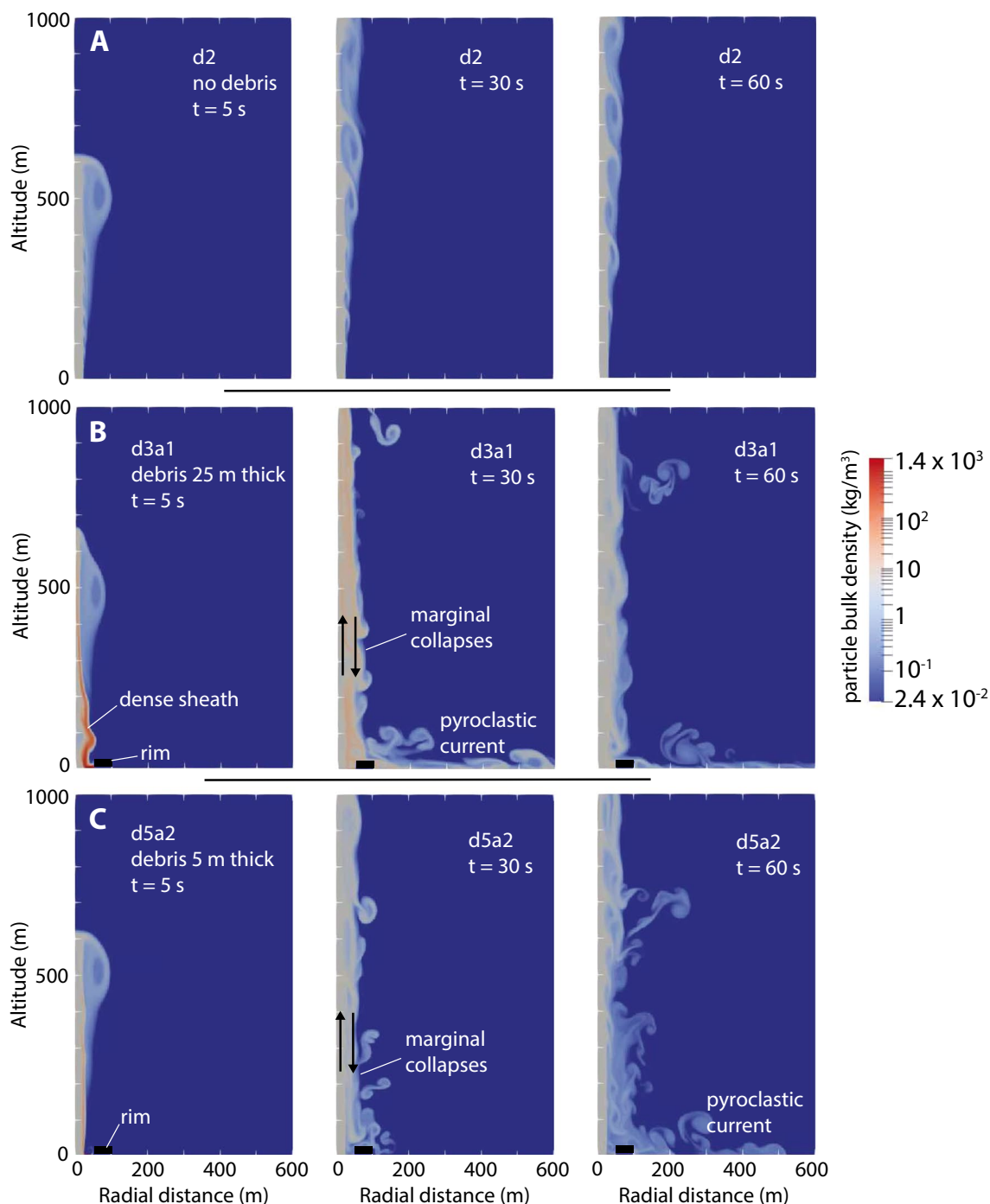
Fig. 2 Comparison of three simulations with vent radius of 25 m, illustrating effects of debris entrainment. Colors represent particle bulk density (product of particle volume fraction and particle density). **a** Snapshots of run d2 at three times, showing development of a jet when there is no debris entrainment. **b** Same eruption conditions but with a 25-m-thick pile of debris initially between 35 and 50 m from symmetry axis (run d3a1). At 5 s, a dense sheath surrounds the jet core at low altitudes due to initial entrainment of debris. By 30 s, the jet has an upward flowing core but collapses from a range of heights along its margin (black arrows show flow directions), which produce a pyroclastic current. **c** Same eruption conditions but with a smaller debris pile, only 5 m thick (run d5a2). Marginal collapses and a pyroclastic current also develop in this case, but by 60 s, much of the debris has been entrained. Note that continued recycling of material that collapses between the rim and vent complicates a potential return to free jet behavior as in part **a**. See Table 2 for simulation conditions

structure, much different from the fountain structure of collapsing columns with no debris interaction. This is "boiling-over" behavior. Maximum collapse heights fluctuate in pulses between ~ 100 and 800 m, much less than the ~ 2 km that would be estimated based upon conversion of initial kinetic energy to potential energy (in the absence of mixing with debris and atmosphere and their effects on mixture density and momentum), illustrating the strong effects of entrainment of highly concentrated debris that has no initial vertical momentum. By 40 s, a significant portion of the debris has escaped the crater as pyroclastic currents, and the eruptive contribution provides some heat that drives development of minor buoyant clouds above the jet. A similar debris volume interacting with a jet from a 50-m-radius vent shows complex marginal collapse from a range of heights due to the dense sheath, but the range of collapses is larger so that some components of pyroclastic currents are sourced from ~ 800 to 900 m altitude while others are sourced as low as ~ 200 m (Fig. 3b).

Larger debris volumes have stronger effects on eruption jets. For example, a jet with vent radius of 25 m interacting with a 2.1×10^6 m³ debris pile entrains so much of the higher particle concentration (denser) debris that it collapses to a low altitude that fluctuates between ~ 100 and 200 m (Fig. 3c), forming a boiling-over phenomenon similar to that in Fig. 3a but with a lower height range for pulses. Resulting pyroclastic currents are relatively cool due to the initial debris temperature and do not form buoyant phoenix clouds. It is unlikely that such an eruption column would ever recover (become buoyant) because the low collapse heights feeding pyroclastic currents and the larger distance to the confining rim mean that most of the debris is destined to be recycled (note that Fig. 2a, c, and b and Fig. 3a and c represent progressively increasing debris volumes for the same eruption conditions). A larger vent radius (100 m) jet interacting with a similar debris volume also shows complex behavior, with tendrils of material collapsing at various heights from the dense sheath of entrained debris (Fig. 3d; see also Valentine and Cole 2021), but the interior portion of the jet, which is composed of the relatively dilute eruptive mixture, forms an open structure several hundred meters high (see also Fig. 3b). This jet structure (see below) is transient like that in Fig. 3c, but with longer time scales between times of low and high jet height. Finally, larger vent radii, which for all other factors being constant also means higher discharge rates, require larger debris volumes to produce marginal collapses.

The jets (especially with large debris volumes; Fig. 3c, d) experience a sort of pinching from debris flowing inward toward the vent along the bottom boundary, which is effectively similar to narrowing the vent while maintaining a constant discharge. Pressure increases in that constricted area, resulting in an overpressure relative to the surrounding atmosphere as the erupting mixture emerges from the inflowing debris, even though the boundary condition at the inlet itself is in equilibrium with the atmosphere. Run d1b models the erupting and debris particles as separate fields in order to illustrate the impacts of this process (Fig. 4; Table 2). The erupting gas-particle mixture forms a jet that alternately widens and then narrows in its lower ~ 400 m (Fig. 4a), while debris particles form a dense sheath around the jet margins (Fig. 4b). Tendrils of mainly debris particles fall toward the ground from altitudes ranging from about 100 to ~ 800 m. Details of gas pressure and vertical speed in the lower 400 m (Fig. 4c, d) illustrate how the jet compresses where it is constricted by inward-flowing debris and then undergoes two expansion-recompression (accompanied by acceleration and deceleration, respectively) and shock structures that are similar to structures that develop in overpressured, gas-only, free jets (Fig. 4e; e.g., Carcano et al. 2014; Koyaguchi et al. 2018). Figure 4 shows snapshots at a single time, and it is important to note that the structures are transient due to the complex interactions between jet, inflowing debris, and recycling of collapsed material. Note that the simulations of Valentine and Cole (2021) had a particle layer initially extending over the vent (inlet) and set the inflow pressure to equal the lithostatic load of the overlying bed while adjusting other parameters to maintain constant mass flux and particle mass fraction from one run to another. The resulting dynamics were similar to those reported here.

Grain size of entrained debris has important effects on eruption jet behavior. For a jet where debris particles are the same small diameter as erupting particles, complex boiling-over phenomenon results. Note that the general phenomena shown in d2a (Fig. 5a) and d2a1 (Fig. 3a), which have identical starting conditions, are similar but different in detail due to the different treatment of particle-gas and particle–particle drag when the debris is treated as a separate particle field (run d2a). The differences between the two figures at 40 s mainly reflect different timing of high pulses in the eruptive jet. In Fig. 5a, the jet has just temporarily risen to an altitude of ~ 800 m and is in the process of falling back down (negative velocities above the ~ 150 m level), while in Fig. 3a, the jet pulse has fallen to its minimum altitude between pulses. Just above the inlet gas velocity is slightly below the inflow speed of 200 m/s at the jet bottom due to influx of debris particles that have initial vertical speed of zero. Speed increases upward to ~ 280 m/s as the gas expands (Fig. 5a) and then decreases again; all of this is related to overpressured jet dynamics due to the choking effect of debris particles flowing over the vent. Up to ~ 150 m altitude, the core of the jet has a negligible debris particle fraction as it is composed nearly entirely of eruptive mixture (Fig. 5a). Debris particles at that altitude form a dense sheath, and flow upward
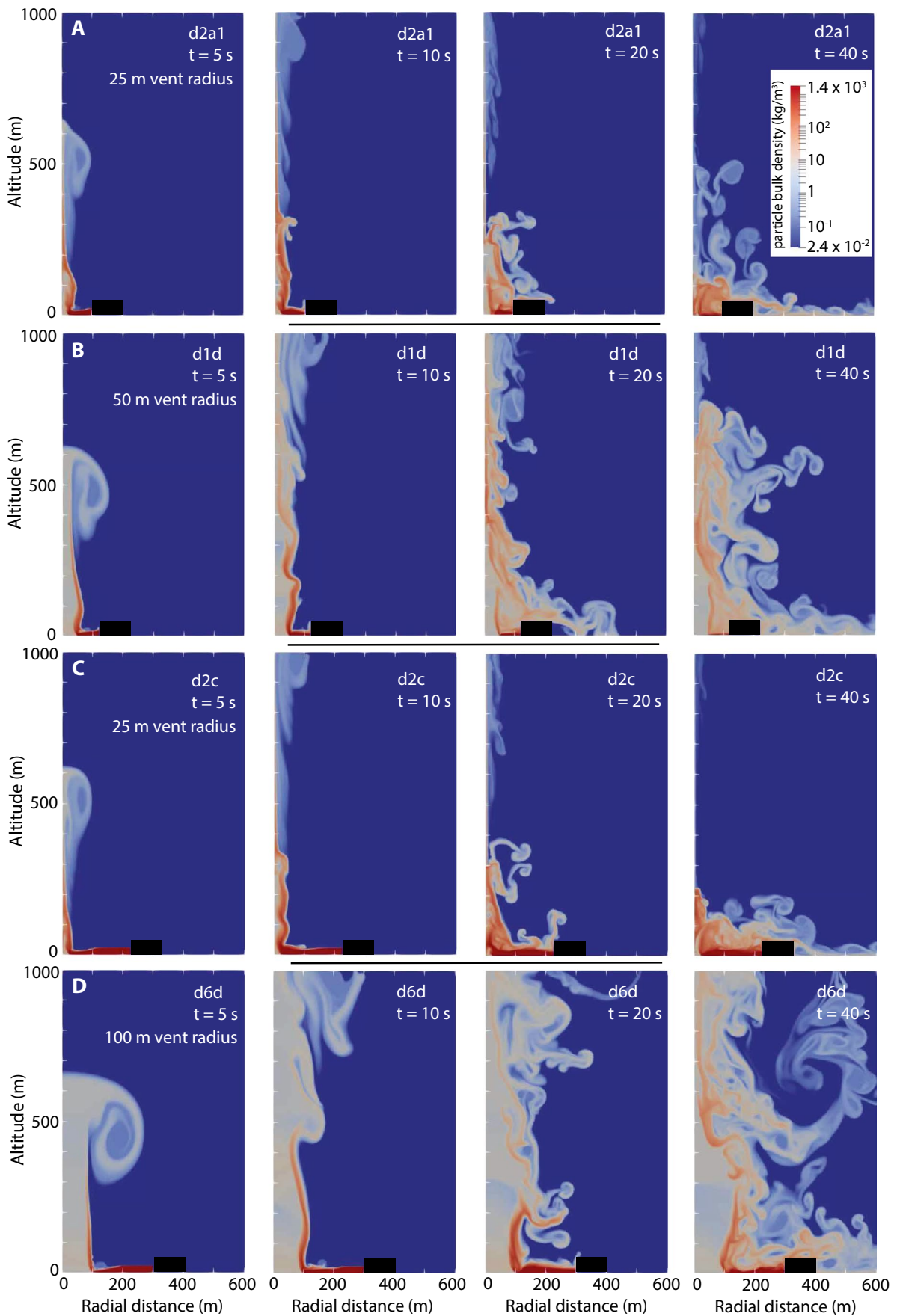
◄**Fig. 3** Snapshots illustrating time evolution of bulk particle density for jets with different vent radii and debris volumes. In all cases, the entrainment of debris results in a dense sheath which causes collapse from the jet margin at a range of heights. **a** Run d2a1, with a 25-m-radius vent and intermediate debris volume (larger than those in Fig. 2), develops a complex boiling-over structure, feeding pyroclastic currents from low altitudes up to ~ 100–800 m, much lower than would be the case if the jet did not interact with debris and collapsed from a height where its initial kinetic energy had been converted to potential energy. **b** Run d1d, which has similar debris volume as in **a** but larger vent radius (50 m), experiences marginal collapses and pyroclastic currents, but due to the much higher discharge rate (higher jet cross section area), it rises to a larger height. Above ~ 600–700 m, the dense sheath has migrated toward the symmetry axis, making the whole jet above that altitude relatively dense. Variations in bulk particle density along the symmetry axis in the lower ~ 400 m reflect expansion and recompression due to the pinching effect of debris flowing over the vent (see Fig. 4). **c** Run d2c, with same conditions as in Fig. 2b and c and in **a** of this figure, but larger debris volume, again producing gargling behavior. **d** Run d6d, with large vent radius of 100 m and large debris volume. Note dilute inner core of jet at 40 s, which experiences overpressured jet dynamics due to pinching effect of debris at the jet base, and tendrils collapsing from the dense sheath at various heights

where the sheath is in contact with the jet core, but downward toward the outer edge of the sheath, which, along with the falling material that had been transported as high as ~ 800 m during a jet pulse, feeds pyroclastic currents. As debris particle size is increased, there is progressively poorer coupling between the erupting particle-gas mixture and coarser debris particles. Compressible flow processes such as compression and deceleration due to choking by incoming debris particles, followed by expansion and acceleration, can be seen, but the jets are collimated with debris particles limited to the outer sheath (Fig. 5a, b; see also Valentine and Cole 2021). This is because the dense, poorly coupled debris sheath inhibits large-scale eddies forming at the jet margin, which are responsible for air entrainment and jet widening (e.g., Fig. 2a). The jet cores maintain relatively high, but variable, speeds up to the domain tops and consist almost entirely of the eruptive gas-particle mixture. Debris particles in the surrounding sheath that are in contact with the inner jet core have high upward speeds, while those on the outer part flow downward and feed pyroclastic currents from a range of heights (Fig. 5b, c). Although downflow occurs all along the outer portion of the sheath, the concentration of particles decreases with height. For example, the sheath in run d2d (1-mm debris particles; Fig. 5b) has particle volume fractions up to ~ 0.02 at 200 m altitude, but only ~ 0.001 at 800 m. The sheath with 1-cm-diameter debris particles (Fig. 5c) is similar at low altitudes but becomes even more dilute by 800 m. Proportions of eruptive particles relative to debris particles increase with height in the sheath. Thus, material falling from greater heights in the sheath will tend to be more dilute and have a higher proportion of eruptive particles compared to sheath material falling from lower altitudes. Pyroclastic currents that are fed by this downflowing material are mainly trapped between the vent and rim for geometries modeled here because of their poor coupling with the gas phase which acts against development of pyroclastic currents, for example compared to the case of fine debris particles (Fig. 5a). Thus, the debris particles are recycled and become an effectively continuous supply of material to feed the dense sheath.

Discussion

The examples described above show a range of eruptive jet behaviors when debris is entrained along jet margins (Fig. 6), compared to the behavior of jets with no debris interaction (Fig. 2a); this complements our growing understanding of eruption column complexities (e.g., Gilchrist and Jellinek 2021). Entrainment of debris produces a dense sheath of granular material around an inner jet core that is dominated by the eruptive gas-particle mixture. This violates the top-hat density model that is common in 1-D eruption column models (see also Houghton et al. 2004). In addition to the relatively high density of the sheath, its velocity structure is such that the inner portion that is in contact with the eruptive gas-particle mixture is dragged upward at the highest speed, while the outer portion is slower and may collapse from a range of heights, except when the debris volume is very small. Both the increased sheath density and its complex velocity profile inhibit the mixing of the eruptive mixture with air that is critical for reducing jet density and achieving buoyancy. Jet structure also depends on how well the entrained debris particles couple with the eruptive gas-particle mixture. Fine-ash size debris particles, such as might represent entrainment of previously erupted ignimbrite, couple with the erupting mixture and cause a complicated, pulsing sort of boiling-over or gargling behavior. An aspect of this coupling is a local reduction of the mixture sound speed where particle concentration is high, promoting compressible flow behavior such as overpressured jet dynamics (Figs. 4, 5a; Kieffer and Sturtevant 1984; Carcano et al. 2014; Valentine and Sweeney 2018; Valentine 2020). In contrast, coarser debris particles do not couple well with the mixture and cause collimation of the eruptive jet within its dense sheath. A caveat is that the modeling here treats eruptive and debris particles each as monodisperse (single particle size and density), although combinations of the two can be bi-disperse if the debris particles are different from the eruptive particles. Of course, in nature, both particle types would be polydisperse, and additional work will explore the effects of debris that comprises combinations of coarse and fine particles.
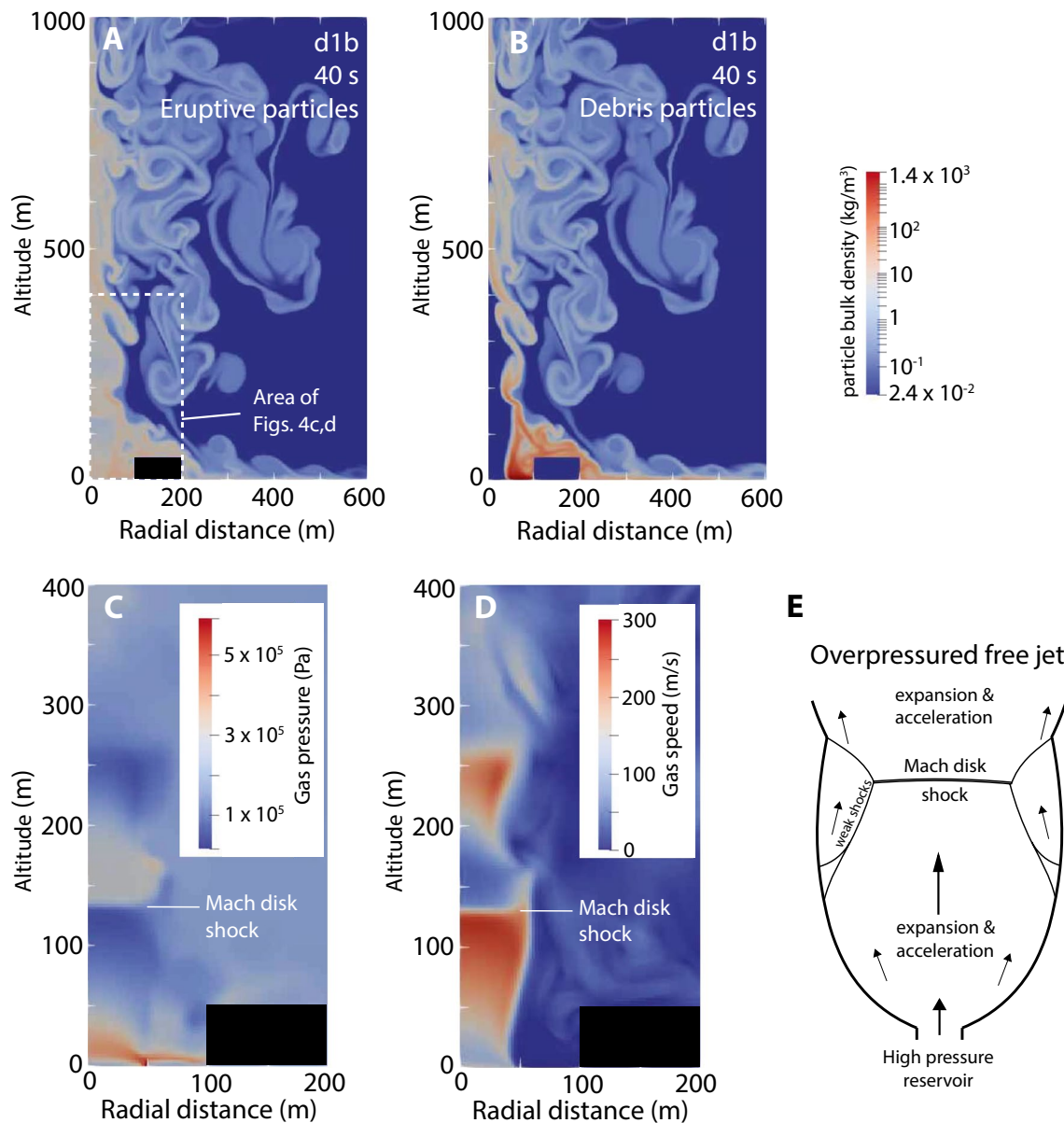
Fig. 4 Snapshots of bulk density of **a** erupting particles and **b** debris particles at 40 s for run d1b (Table 2). In this simulation, the two particle types have identical properties but are modeled as separate fields in order to illustrate the complexity of the debris entrainment process. Note that the eruptive mixture dominates the jet interior, while the debris particles are focused around the outer margin of the jet up to an altitude of ~ 400 m (dense sheath). Snapshots showing **c** gas pressure and **d** gas speed (magnitude of velocity) in the lower 400 m of the jet illustrate expansion, recompression, and corresponding acceleration and deceleration caused by overpressure where debris pinches the jet. Note that the rapid pressure increase (velocity decrease) labeled Mach disk shock in **c** and **d** is not strictly speaking a shock in the numerical simulations because it is spread over a few cells. **e** These dynamics are similar to those of an overpressured (underexpanded) free jet (modified from Valentine and Sweeney 2018)

Larger debris volumes, for a given discharge rate and vent size, have stronger and longer-lasting effects on the jets. If the debris volume is small relative to the eruptive discharge rate (e.g., Fig. 2c, where debris volume is equal to ~ 16 s of discharge), it might cause temporary marginal collapses. For very small debris volumes, such as run d6b (Table 1) where debris is equivalent to only ~ 3 s of the discharge rate

produce, a dense sheath is dragged upward and mixed into the jet as it approaches the top of the 1-km-high domain, with no significant marginal collapses.

Field studies of proximal deposits from large, sustained explosive eruptions indicate simultaneous generation of buoyant plumes (fallout deposits) and pyroclastic currents (ignimbrites and pyroclastic surge deposits), and hybrids

of the two processes (e.g., Dowey and Williams 2022), that were fed by collapses at different elevations in the eruption column (Fierstein and Hildreth 1992). Some authors have related this to entrainment of lithic debris and/or earlier-erupted pyroclastic material and to lateral variability in the composition of erupting juvenile material, causing collapses of a column margin (e.g., Wilson and Walker 1985; Wilson and Hildreth 1997; Houghton et al. 2004; Hildreth and Fierstein 2012). The modeling presented here demonstrates how pyroclastic currents may be fed by collapses from a range of altitudes while the eruptive mixture flows upward within the jet core (Fig. 5). While this paper only addresses the lower 1 km of eruptive jets, and therefore does not show whether a buoyant plume can develop from the core of a jet while collapses occur along its margins, Valentine and Cole (2021) do illustrate a larger-scale domain where the dense sheath extends to 3.5 km altitude, and a buoyant or near-buoyant mixture emerges from that height. More modeling is needed, but this suggests that relatively poorly coupled dense sheath particles, and resulting collimated jets (e.g., Fig. 5b, c), could produce simultaneous buoyant plumes and collapse-fed pyroclastic currents.

The term boiling-over (or boil-over) has been used to describe a low fountaining process that feeds low-energy pyroclastic currents (see, for example, Brand et al. 2023). Rader et al. (2015) reviewed previous uses of that term based upon eruption observations, deposit characteristics, and modeling. They proposed that it applies to high discharge rate eruptions with low exit velocities and low volatile contents that result in low fountains, little buoyant plume activity, and short-runout, concentrated pyroclastic currents. Koyaguchi et al. (2018) discussed how low exit velocities can also be caused by decompression of an erupting mixture inside a crater. The modeling reported here indicates that entrainment of lithic debris and/or recycled pyroclasts along the margins of an eruptive jet can also produce boiling-over dynamics, even with modestly high erupting gas content (4 wt% in my simulations). In particular, recycling might be promoted for situations with craters that are closed or have restricted outlets. Rader et al. (2015) used thermal demagnetization to estimate emplacement temperatures of deposits from boiling-over-produced pyroclastic currents at Tungurahua volcano (Ecuador). Their data, along with other observations such as varying degrees of wood charring in the deposits, indicate heterogeneous emplacement temperatures. Rader et al. (2015) suggested that cooling of the eruptive mixtures by contact with air entrained by the pyroclastic currents prevented heating of lithic clasts and promoted quenching of juvenile clasts. Locally, low emplacement temperatures may also have resulted in part from entrainment of cold debris and recycled pyroclasts. Lithic material is abundant in the

Tungurahua deposits, a few tens of volume percent (Doulliet et al. 2013); such lithic contents are consistent with entrainment of substantial debris as the eruptive jet emerged from its vent.

This paper shows how entrainment of debris into an erupting jet can result in pyroclastic currents, even when vent diameter, exit velocity, and gas content (eruptive mixture density) do not change and would otherwise combine to produce a buoyant column in the absence of debris. Even entrainment of relatively small volumes of debris can result in collapses of the dense sheath, at least temporarily. It seems likely that increased stratification of fall deposits as their lithic content increases (see Introduction) is related to transient behavior associated with a developing dense sheath of entrained debris. For example, if a buoyant column has been established, but an avalanche feeds a small volume of lithic debris into the column, a temporary dense sheath would develop and reduce air entrainment in the lower jet (gas-thrust) portion of the column, potentially temporarily reducing the column height. For very small entrained volumes that mix into the jets, both the increased mass loading (relative to vent discharge) and low temperature of lithic debris would have additional effects on plume height. Bear et al. (2009) presented detailed data on pyroclastic deposits of the Sutri eruption in central Italy. Although there were many processes involved in that complex eruption sequence, one of them involved column collapse (or partial collapse) due to overloading with coarse and dense lithic material as evidenced by widespread lithic breccias associated with ignimbrites (see also Simmons et al. 2016). My results show some of the details involved in this process of pyroclastic current generation due to lithic entrainment.

Conclusions

This study has taken a simple approach, within a multiphase fluid dynamic framework, to explore the effects of entrainment of granular debris into sustained volcanic jets such as would, in the absence of debris interaction, produce buoyant eruption columns (Fig. 6). The results indicate that debris is not immediately, homogeneously mixed into a jet but instead forms a dense sheath or collar around the jet. The inner portion of the dense sheath is dragged upward by the erupting mixture, while less momentum is imparted to the outer portion. The presence of the sheath of entrained debris violates some of the key assumptions that comprise standard eruption column models, such as the top-hat profile for density and velocity that is commonly used in 1-D models. The dense sheath inhibits entrainment of air into the eruptive mixture, which may explain signs of column instability such as increased stratification in fallout deposits
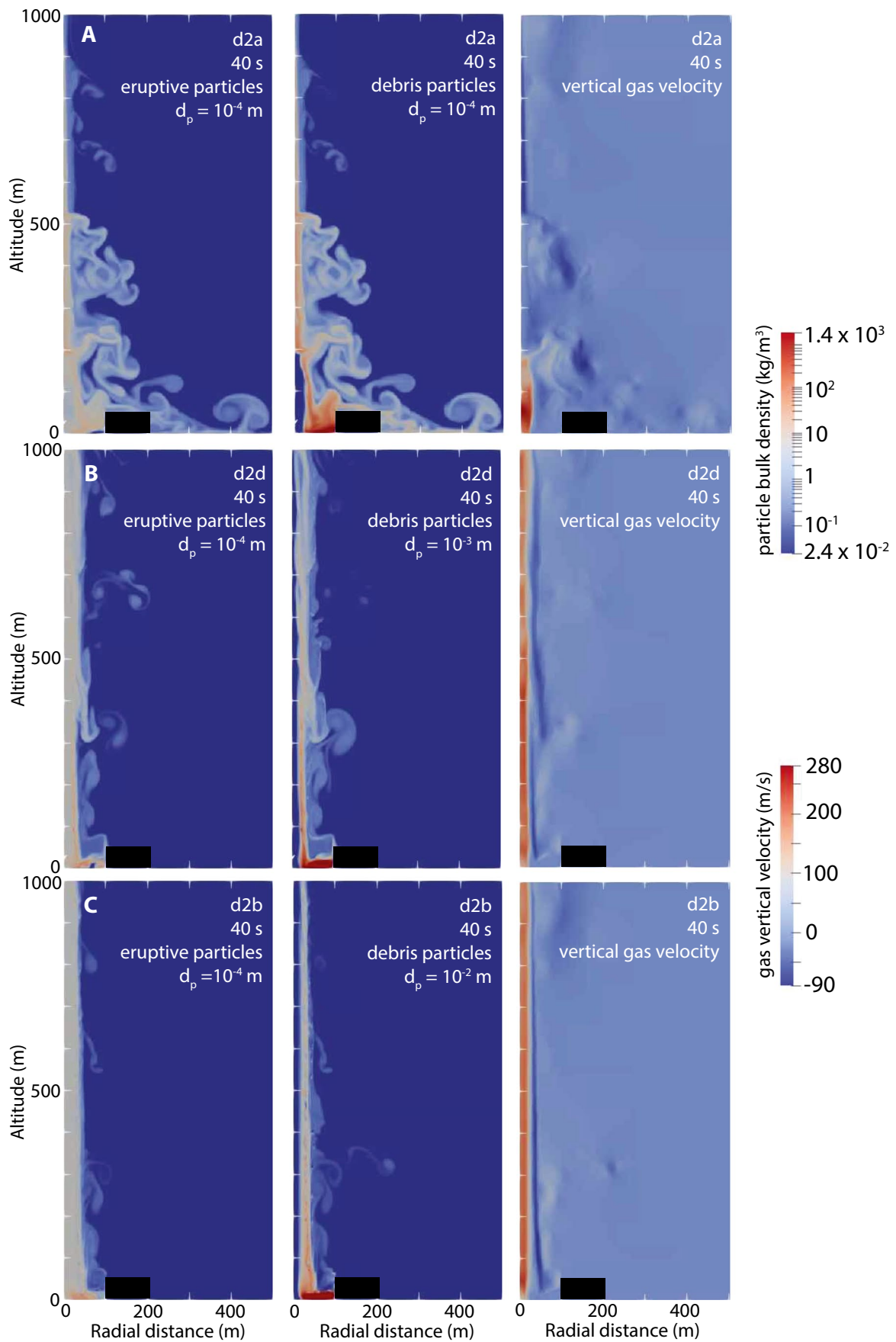
◀**Fig. 5** Snapshots from three simulations with different debris particle sizes, at 40 s, showing bulk density of eruptive particles (left-hand column), debris particles (center), and vertical component of gas velocity (right-hand column). **a** Eruptive and debris particles the same size ($d_p = 10^{-4}$ m, where d_p is the particle diameter), showing collapsing tendrils and good coupling of all particles and gas. **b** Debris particles $d_p = 10^{-3}$ m, showing collimated jet with debris particles remaining in the dense sheath and falling back from a range of heights, and distinction between upward flow (red) in jet core and downward flow (dark blue) along margins in the gas velocity plot. **c** Debris particles with $d_p = 10^{-2}$ m show similar jet collimation with upward flow in core and downward flow along margin. In both **b** and **c**, the downward marginal flow is dominated by the coarser debris particles

when lithic content increases. Furthermore, the dense sheath can collapse from a range of elevations to feed pyroclastic currents which would be expected to have different initial kinetic energies as they impact the ground. The transition from fallout-producing buoyant column to collapsing behavior can be related to debris entrainment without any changes in primary eruption parameters such as vent size, exit velocity, or gas content. Boiling-over behavior, an extreme form of gargle dynamics (Valentine and Cole 2021), can also be caused by entrainment of large volumes of debris, including recycled previously erupted material. When entrained debris is relatively fine-grained such that it can couple well with the erupting mixture, complex overpressured jet processes can occur due to the pinching effect of debris at the base of the jet, although these processes are highly transient. Increasingly coarse debris can cause collimation of the jet within the sheath of entrained material (Fig. 6).

The results presented here suggest that accounting for the effects of debris entrainment is likely important for theoretical assessment of many natural eruption sequences. Additionally, hazard scenarios at volcanoes that potentially could experience sub-Plinian to Plinian activity might benefit from exploration of the effects of debris entrainment and recycling. Violent Strombolian activity, consisting of smaller scale sustained eruption columns (Pioli et al. 2008; Valentine and Gregg 2008), could also experience the modeled phenomena, for example as scoria avalanches from crater

walls into a vent. Additional work should explore processes that might result from polydisperse debris mixtures, extend the modeling to higher altitudes for some scenarios such as the collimated jets in order to assess potential transitions to buoyant behavior, and conduct three-dimensional modeling to capture potential circumferential variability such as might result from introduction of debris on one side of a jet but not the other.

Appendix

Modeling approach

The governing equations are conservation of mass, momentum, and energy for a carrier gas phase and for one or two fields of dispersed particles. The equations are written in an Eulerian framework for both the gas and the particle fields, which are treated as overlapping continua with volume fractions within a control volume that sum to unity. Gas and particle fields interact with each other through momentum transfer (drag) and heat transfer. More details can be found in Benyahia et al. (2012), Sweeney and Valentine (2017), and Valentine and Sweeney (2018). The governing equations are as follows (nomenclature in Table 3):
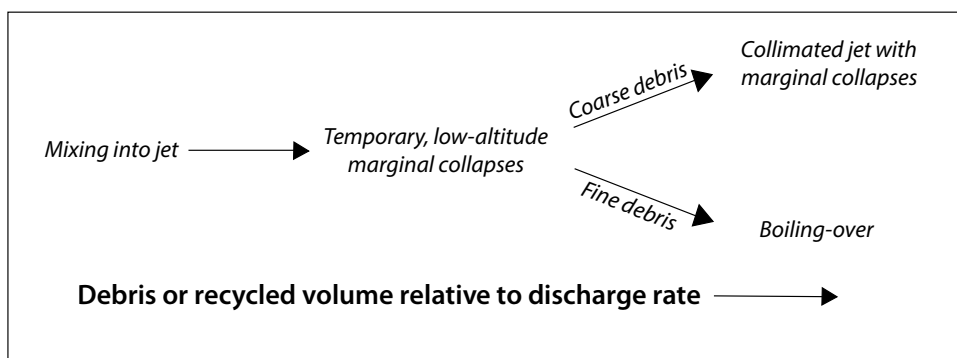
$$\frac{\partial}{\partial t}\left(\epsilon_g \rho_g\right) + \frac{\partial}{\partial x_j}\left(\epsilon_g \rho_g U_{gj}\right) = 0. \tag{1}$$

$$\frac{\partial}{\partial t}\left(\epsilon_m \rho_m\right) + \frac{\partial}{\partial x_j}\left(\epsilon_m \rho_m U_{mj}\right) = 0. \tag{2}$$

$$\frac{\partial}{\partial t}\left(\epsilon_g \rho_g U_{gi}\right) + \frac{\partial}{\partial x_j}\left(\epsilon_g \rho_g U_{gj} U_{gi}\right) = -\epsilon_g \frac{\partial P_g}{\partial x_i} + \frac{\partial \tau_{gij}}{\partial x_j} - \sum_{m=1}^{M} I_{gmi} + \epsilon_g \rho_g g_i. \tag{3}$$

$$\frac{\partial}{\partial t}\left(\epsilon_m \rho_m U_{mi}\right) + \frac{\partial}{\partial x_j}\left(\epsilon_m \rho_m U_{mj} U_{mi}\right) = -\epsilon_m \frac{\partial P_g}{\partial x_i} + \frac{\partial \tau_{mij}}{\partial x_j} + I_{gmi} - \sum_{l=1}^{M} I_{mli} + \epsilon_m \rho_m g_i. \tag{4}$$

Fig. 6 Diagram qualitatively summarizing jet behaviors as a function of debris (or recycled) volume relative to eruptive discharge rate. As debris volume increases for a given discharge rate, behavior depends also on the debris grain size which can result in boiling-over behavior (fine particles) or collimated jets with marginal collapses (coarse particles)

Mixing into jet ⟶ *Temporary, low-altitude marginal collapses*

Coarse debris ➤ *Collimated jet with marginal collapses*

Fine debris ➤ *Boiling-over*

Debris or recycled volume relative to discharge rate ⟶

Table 3 Notation for Eqs. 1–6

Symbol	Definition
C_{pm}	Specific heat of the mth particle phase; J/kg K
C_{pg}	Specific heat of the gas phase; J/kg K
g_i	Acceleration due to gravity; m/s^2
i, j, k	Subscripts for identifying vector and tensor components; if there are multiple subscripts, these indices appear at the end of the list of subscripts and summation convention is implied only for these indices
I_{gmi}	Momentum transfer between the gas and the mth phases due to interphase drag force; N/m^3
I_{mli}	Momentum transfer between the mth and the lth phases due to interphase drag force; N/m^3
M	Total number of solid phases
P_g	Gas phase pressure; Pa
q_{gj}	Conductive heat flux in the gas phase; J/m^2 s
q_{mj}	Conductive heat flux in the mth phase; J/m^2 s
t	Time; s
T_g	Thermodynamic temperature of the gas phase; K
T_m	Thermodynamic temperature of the mth solids phase; K
T_{Rg}	Fluid phase radiation temperature; K
T_{Rm}	Solid phase m radiation temperature; K
U_{gj}	J^{th} component of the gas phase velocity; m/s
U_{mj}	J^{th} component of the mth solids phase velocity; m/s
x_j	J^{th} coordinate direction; m
γ_{gm}	Gas–solid heat transfer coefficient; J/m^3 K s
γ_{Rm}	Radiative heat transfer coefficient for the mth phase; J/m^3 K^4 s
ϵ_g	Volume fraction of the gas phase
ϵ_m	Volume fraction of the mth solids phase
ρ_g	Material density of the gas phase; kg/m^3
ρ_m	Material density of the mth solids phase; kg/m^3
τ_{gij}	Stress tensor of the gas phase; Pa
τ_{mij}	Stress tensor of the mth phase; Pa

$$\epsilon_g \rho_g C_{pg} \left[\frac{\partial T_g}{\partial t} + U_{gi} \frac{\partial T_g}{\partial x_j} \right] = -\frac{\partial q_{gj}}{\partial x_j} + \sum_{m=1}^{M} \gamma_{gm}(T_m - T_g) + \gamma_{Rg}\left(T_{Rg}^4 - T_g^4\right). \tag{5}$$

$$\epsilon_m \rho_m C_{pm} \left[\frac{\partial T_m}{\partial t} + U_{mj} \frac{\partial T_m}{\partial x_j} \right] = -\frac{\partial q_{mj}}{\partial x_j} - \gamma_{gm}(T_m - T_g) + \gamma_{Rm}\left(T_{Rm}^4 - T_m^4\right). \tag{6}$$

Constitutive models that describe interphase heat and momentum transfer, and intraphase heat transfer and stress, are found in Syamlal et al. (1993), Syamlal and Pannala (2011), Benyahia et al. (2012), and Sweeney and Valentine (2015, 2017). Valentine and Sweeney (2018) include information related to model validation. In this and similar gas-particle multiphase approaches, stresses within the particle phase (Eq. 4) are modeled as a function of the so-called granular temperature (a.k.a. granular energy), which is a measure of the fluctuation of particle velocities. Here, I use an algebraic approximation for granular temperature rather than a full conservation equation (see Benyahia et al 2012; Breard et al. 2019; Valentine 2020). Additional volcanological applications of the MFIX code can be found in Dartevelle (2004), Dartevelle et al. (2004), Dufek and Bergantz (2007a, b), Dufek and Manga (2008), Dufek et al. 2009), and Breard et al. (2018, 2019).

References

Andrews RG, White JDL, Dürig T, Zimanowski B (2014) Discrete blasts in granular material yield two-stage process of cavitation and granular fountaining. Geophys Res Lett 41:422–428. https://doi.org/10.1002/2013GL058526

Andrews RG, White JDL, Dürig T, Zimanowski B (2016) Simulating maar-diatreme volcanic systems in bench-scale experiments. Geol Soc London 173:265–281. https://doi.org/10.1144/jgs2015-073

Anilkumar AV, Sparks RSJ, Sturtevant B (1993) Geological implications and applications of high-velocity two-phase flow experiments. J Volcanol Geotherm Res 56:145–160. https://doi.org/10.1016/0377-0273(93)90056

Bear AN, Cas RAF, Giordano G (2009) The implications of spatter, pumice and lithic clast rich proximal co-ignimbrite lag breccias on the dynamics of caldera forming eruptions: the 151 ka Sutri eruption, Vico Volcano, Central Italy. J Volcanol Geotherm Res 181:1–24. https://doi.org/10.1016/j.jvolgeores.2008.11.032

Benyahia S, Syamlal M, O'Brien TJ (2012) Summary of MFIX Equations 2012–1. https://mfix.netl.doe.gov/doc/mfix-archive/mfix_current_documentation/MFIXEquations2012-1.pdf. Accessed 20 April 2023

Brand BD, Pollock N, Vallance JW, Esposti Ongaro T, Roche O, Trolese M, Giordano G, Marshall AA, Criswell SW (2023) Advances in our understanding of pyroclastic current behavior from the 1980 eruption sequence of Mount St. Helens volcano (Washington) USA. Bull Volc 85:24. https://doi.org/10.1007/s00445-022-01617

Breard ECP, Dufek J, Lube G (2018) Enhanced mobility of concentrated pyroclastic density currents: an examination of a self-fluidization mechanism. Geophys Res Lett 45:654–664. https://doi.org/10.1002/2017GL075759

Breard ECP, Dufek J, Roche O (2019) Continuum modeling of pressure-balanced and fluidized granular flows in 2-D: comparison with glass bead experiments and implications for concentrated pyroclastic density currents. J Geophys Res Sol Earth 124:5557–5583. https://doi.org/10.1029/2018JB016874

Burcat A, Ruscic B (2005) Third Millennium ideal gas and condensed phase thermochemical database for combustion with updates from active thermochemical tables. Report ANL-05/20 TAE 960 Argonne National Laboratory Argonne IL USA

Carcano S, Esposti Ongaro T, Bonaventura L, Neri A (2014) Influence of grain-size distribution on the dynamics of underexpanded volcanic jets. J Volcanol Geotherm Res 285:60–80. https://doi.org/10.1016/j.volgeores.2014.08.003

Cerminara M, Esposti Ongaro T, Berselli LC (2016) ASHEE-1.0: a compressible, equilibrium-Eulerian model for volcanic ash plumes. Geosci Model Dev 9:697–730. https://doi.org/10.5194/gmd-9-697-2016

Dartevelle S (2004). Numerical modeling of geophysical granular flows: 1. a comprehensive approach to granular rheologies and geophysical multiphase flows. Geochem Geophys Geosys 5:Q08003. https://doi.org/10.1029/2003GC000636

Dartevelle S, Valentine GA (2007) Transient multiphase processes during the explosive eruption of basalt through a geothermal borehole (Námafjall, Iceland, 1977) and implications for natural volcanic flows. Earth Planet Sci Lett 262:363–384. https://doi.org/10.1016/j.epsl.2007.07.053

Dartevelle S, Rose WI, Stix J, Kelfoun K, Vallance JW (2004) Numerical modeling of geophysical granular flows: 2 computer simulations of plinian clouds and pyroclastic flows and surges. Geochem Geophys Geosys 5:Q08004. https://doi.org/10.1029/2003GC000637

Di Muro A, Neri A, Rosi M (2004) Contemporaneous convective and collapsing eruptive dynamics: the transitional regime of explosive eruptions. Geophys Res Lett 31:2001–2004

Di Muro A, Rosi M, Aguilera E, Barbieri R, Massa G, Mondula F, Pieri F (2008) Transport and sedimentation dynamics of transitional explosive eruption columns: the example of the 800 BP Quilotos plinian eruption (Ecuador). J Volcanol Geotherm Res 174:307–324. https://doi.org/10.1016/j.jvolgeores.2008.03.002

Doulliet GA, Tsang-Hin-Sun É, Kueppers U, Letort J, Pacheco DA, Goldstein F, Von Aulock F, Lavallée Y, Hanson JB, Bustillos J, Robin C, Ramón P, Hall M, Dingwell DB (2013) Sedimentology and geomorphology of the deposits from the August 2006 pyroclastic density currents at Tungurahua volcano. Ecuador Bull Volcanol 75:765. https://doi.org/10.1007/s00445-013-0765-7

Dowey N, Williams R (2022) Simultaneous fall and flow during pyroclastic eruptions: a novel proximal hybrid facies. Geology 50:1187–1191. https://doi.org/10.1130/G50169.1

Druitt TH (1985) Vent evolution and lag breccia formation during the Cape Riva eruption of Santorini, Greece. J Geol 93:439–454

Druitt TH, Bacon CR (1986) Lithic breccia and ignimbrite erupted during the collapse of Crater Lake Caldera, Oregon. J Volcanol Geotherm Res 29:1–32

Dufek J, Bergantz GW (2007a) Dynamics and deposits generated by the kos plateau tuff eruption: controls of basal particle loss on pyroclastic flow transport. Geochem Geophys Geosys 8:Q12007. https://doi.org/10.1029/2007GC001741

Dufek J, Bergantz GW (2007b) Suspended load and bed-load transport of particle-laden gravity currents: the role of particle-bed interaction. Theor Comp Fluid Dyn 21:119–145. https://doi.org/10.1007/s00162-007-0041-6

Dufek J, Manga M (2008) In situ production of ash in pyroclastic flows. J Geophys Res Sol Earth 113:B09207. https://doi.org/10.1029/2007JB005555

Dufek J, Wexler J, Manga M (2009) Transport capacity of pyroclastic density currents: experiments and models of substrate-flow interaction. J Geophys Res Sol Earth 114:B11203. https://doi.org/10.1029/2008JB006216

Fierstein J, Hildreth W (1992) The plinian eruptions of 1912 at Novarupta, Katmai National Park, Alaska. Bull Volcanol 54:646–684

Gilchrist JT, Jellinek AM (2021) Sediment waves and the gravitational stability of volcanic jets. Bull Volcanol 83:64. https://doi.org/10.1007/s00445-021-01422-1

Glaze LS, Baloga SM (1996) Sensitivity of buoyant plume heights to ambient atmospheric conditions: implications for volcanic eruption columns. J Geophys Res 101:1529–1540

Graettinger AH, Valentine GA, Sonder I, Ross P-S, White JDL, Taddeucci J (2014) Maar-diatreme geometry and deposits: subsurface blast experiments with variable explosion depth. Geochem Geophys Geosys 15. https://doi.org/10.1002/2013GC005198

Hildreth W, Fierstein J (2012) The Novarupta-Katmai eruption of 1912 - largest eruption of the twentieth century: centennial perspectives. US Geol Surv Prof Pap 1791:259. https://doi.org/10.3133/pp1791

Houghton BF, Wilson CJN, Fierstein J, Hildreth W (2004) Complex proximal deposition during the Plinian eruptions of 1912 at Novarupta, Alaska. Bull Volcanol 66:95–133. https://doi.org/10.1007/s00445-003-0297-7

Kieffer SW, Sturtevant B (1984) Laboratory studies of volcanic jets. J Geophys Res 89:8253–8268

Koyaguchi T, Suzuki YJ, Takeda K, Inagawa S (2018) The condition of eruption column collapse: 2. three-dimensional numerical simulations of eruption column dynamics. J Geophys Res Sol Earth 123:7483–7508. https://doi.org/10.1029/2017JB015259

Marble FE (1970) Dynamics of dusty gases. Ann Rev Fluid Mech 2:397–446

Mastin LG (2007) A user-friendly one-dimensional model for wet volcanic plumes. Geochem Geophys Geosys 8:Q03014. https://doi.org/10.1029/2006GC001455

Neri A, Dobran F (1994) Influence of eruption parameters on the thermofluid dynamics of collapsing volcanic columns. J Geophys Res 99:11833–11857

Ogden DE, Glatzmaier GA, Wohletz KH (2008) Effects of vent overpressure on buoyant eruption columns: implications for plume stability. Earth Planet Sci Lett 268:283–292. https://doi.org/10.1016/j.epsl.2008.01.014

Pioli L, Erlund E, Johnson E, Cashman K, Wallace P, Rosi M, Delgado Granados H (2008) Explosive dynamics of violent

Strombolian eruptions: the eruption of Parícutin volcano 1943–1952 (Mexico). J Volcanol Geotherm Res 271:359–368. https://doi.org/10.1016/j.epsl.2008.04.026

Rader E, Geist D, Geissman J, Dufek J, Harpp K (2015) Hot clasts and cold blasts: thermal heterogeneity in boiling-over pyroclastic density currents. In: Ort MH, Porreca M, Geisman JW (eds), The use of paleomagnetism and rock magnetism to understand volcanic processes. Geol Soc London Sp Pub 396:67–86. https://doi.org/10.1144/SP396.16

Rosi M, Vezzoli L, Castelmenzano A, Grieco G (1999) Plinian pumice fall deposit of the campanian ignimbrite eruption (Phlegraean Fields, Italy). J Volcanol Geotherm Res 91:179–198

Ross P-S, White JDL, Zimanowski B, Büttner R (2008a) Multiphase flow above explosion sites in debris-filled volcanic vents: insights from analogue experiments. J Volcanol Geotherm Res 178:104–112

Ross P-S, White JDL, Zimanowski B, Büttner R (2008b) Rapid injection of particles and gas into non-fluidized granular material, and some volcanological implications. Bull Volcanol 70:1151–1168. https://doi.org/10.1007/s00445-008-02301

Scarpati C, Perrotta A (2016) Stratigraphy and physical parameters of the plinian phase of the campanian ignimbrite eruption. Geol Soc Am Bull 128:1147–1159. https://doi.org/10.1130/B31331.1

Simmons JM, Cas RAF, Druitt TH, Folkes CB (2016) Complex variations during a caldera-forming Plinian eruption, including precursor deposits, thick pumice fallout, co-ignimbrite breccias and climactic lag breccias: THE 184 ka Lower pumice 1 eruption sequence, Santorini, Greece. J Volcanol Geotherm Res 324:200–219. https://doi.org/10.1016/j.volgeores.2016.05.013

Sparks RSJ, Bursik MI, Carey SN, Gilbert JS, Glaze LS, Sigurdsson H, Woods AW (1997) Volcanic plumes. Wiley 590

Suzuki YJ, Koyaguchi T (2012) 3-D numerical simulation of eruption column collapse: effects of vent size on pressure-balanced jet/plumes. J Volcanol Geotherm Res 221–222:1–13. https://doi.org/10.1016/j.volgeores.2012.01.013

Suzuki YJ, Koyaguchi T, Ogawa M, Hachisu I (2005) A numerical study of turbulent mixing in eruption clouds using a three-dimensional fluid dynamics model. J Geophys Res 110:B08201. https://doi.org/10.1029/2004JB003460

Suzuki-Kamata K, Kamata H, Bacon CR (1993) Evolution of the caldera-forming eruption at Crater Lake, Oregon, indicated by component analysis of lithic fragments. J Geophys Res Sol Earth 98:14059–14074. https://doi.org/10.1029/93JB00934

Sweeney MR, Valentine GA (2015) Transport and mixing dynamics from explosions in debris-filled volcanic conduits: numerical results and implications for maar-diatreme volcanoes. Earth Planet Sci Lett 425:64–76. https://doi.org/10.1016/j.epsl.2015.05.038

Sweeney MR, Valentine GA (2017) Impact zone dynamics of dilute mono-and polydisperse jets and their implications for initial conditions of pyroclastic density currents. Phys Fluids 29:093304. https://doi.org/10.1063/1/5004197

Sweeney MR, Grosso ZS, Valentine GA (2018) Topographic controls on a phreatomagmatic maar-diatreme eruption (Holocene Dotsero volcano, Colorado, USA): field and numerical results. Bull Volcanol 80:78. https://doi.org/10.1007/s00445-018-1253-x

Syamlal M, Pannala S (2011) Multiphase continuum formulation for gas-solids reacting flows. In: Pannala S, Syamlal M, O'Brien TJ (eds), Computational gas-solids flows and reacting systems: theory methods and practice. Hershey Pennsylvania IGI Global: 1–65

Syamlal M, Rogers W, O'Brien TJ (1993) MFIX documentation theory guide. Technical Note DOE/METC-94/1004, NTIS/DE94000087

US Dept Energy Morgantown Energy Technology Center West Virginia 52

Syamlal M, Musser J, Dietiker J-F (2017) Two-fluid model in MFIX. In: Michaelides EE, Crowe CT, Schwarzkopf JD (eds) Multiphase flow handbook, 2nd edn. CRC Press, Boca Raton, pp 242–275

Taddeucci J, Wohletz KH (2001) Temporal evolution of the Minoan eruption (Santorini, Greece), as recorded by its Plinian fall deposit and interlayered ash flow beds. J Volcanol Geotherm Res 109:209–317

Valentine GA (2020) Initiation of dilute and concentrated pyroclastic currents from collapsing mixtures and origin of their proximal deposits. Bull Volcanol 82:20. https://doi.org/10.1007/s00445-020-1366-x

Valentine GA, Cole MA (2021) Explosive caldera-forming eruptions and debris-filled vents: gargle dynamics. Geology 49:1240–1244. https://doi.org/10.1130/G48995

Valentine GA, Gregg TKP (2008) Continental basaltic volcanoes – processes and problems. J Volcanol Geotherm Res 177:857–873. https://doi.org/10.1016/j.jvolgeores.2008.01.050

Valentine GA, Sweeney MR (2018) Compressible flow phenomena at inception of lateral density currents fed by collapsing gas-particle mixtures. J Geophys Res Sol Earth 123:1286–1302. https://doi.org/10.1002/2017JB015129

Valentine GA, Wohletz KH (1989) Numerical models of Plinian eruption columns and pyroclastic flows. J Geophys Res 94:1867–1887

Valentine GA, Graettinger AH, Sonder I (2014) Explosion depths for phreatomagmatic eruptions. Geophys Res Lett 41:3045–3051. https://doi.org/10.1002/2014GL060096

Valentine GA, Graettinger AH, Macorps E, Ross P-S, White JDL, Döhring E, Sonder I (2015) Experiments with vertically- and laterally-migrating subsurface explosions with applications to the geology of phreatomagmatic and hydrothermal explosion craters and diatremes. Bull Volcanol 77:15. https://doi.org/10.1007/s00445-015-0901-7

Valentine GA, Palladino DM, DiemKaye K, Fletcher C (2019) Lithic-rich and lithic-poor ignimbrites and their basal deposits: Sovana and Sorano formations (Latera caldera, Italy). Bull Volcanol 81:29. https://doi.org/10.1007/s00445-019-1288-7

Walker GPL (1981) Plinian eruptions and their products. Bull Volcanol 44:223–240

Wilson CJN, Hildreth W (1997) The Bishop Tuff: new insights from eruptive stratigraphy. J Geol 105:407–439

Wilson CJN, Walker GPL (1985) The Taupo eruption, New Zealand I. General aspects. Phil Trans R Soc Lond 314:199–228

Wilson L, Sparks RSJ (1980) Explosive volcanic eruptions - IV. The control of magma properties and conduit geometry on eruption column behavior. Geophys J Internat 63:117–148. https://doi.org/10.1111/j.1365-246X.1980.tb02613.x

Woods AW (1988) The fluid dynamics and thermodynamics of Plinian eruption columns. Bull Volcanol 50:169–193

Yasuda Y, Suzuki-Kamata K (2018) The origin of a coarse lithic breccia in the 34 ka caldera-forming Sounkyo eruption, Taisetsu volcano group, central Hokkaido, Japan. J Volcanol Geotherm Res 357:287–305. https://doi.org/10.1016/j.jvolgeores.2018.04.017